Photodiagnosis and Photodynamic Therapy 25 (2019) 35–42

Contents lists available at ScienceDirect

Photodiagnosis and Photodynamic Therapy

journal homepage: www.elsevier.com/locate/pdpdt

# Photophysical properties and *in vitro* photocytotoxicity of disodium salt 2.4-di(alpha-methoxyethyl)-deuteroporphyrin-IX (Dimegine)

Dadeko A.V.[a,*], Lilge L.[b,c], Kaspler P.[c], Murav'eva T.D.[a], Starodubtcev A.M.[a], Kiselev V.M.[a], Zarubaev V.V.[d], Ponomarev G.V.[e]

[a] Joint-stock company "Vavilov State Optical Institute", 199053, 5/2 Kadetskaya line, Saint Petersburg, Russia
[b] Department of Medical Biophysics, University of Toronto, M5G 1L7, 101 College Street, Suite 15-701, Toronto, Ontario, Canada
[c] Princess Margaret Cancer Centre, University Health Network, M5G 2M9, 610 University Ave, Toronto, Ontario, Canada
[d] Pasteur Institute of Epidemiology and Microbiology, 14 Mira St., 197101, St. Petersburg, Russian Federation
[e] Institute of Biomedical Chemistry, 119435, 10c8 Pogodinskaya St., Moscow, Russia

ARTICLE INFO

*Keywords:*
photosensitizer
singlet oxygen quantum yield
fluorescence quantum yield
Dimegine
photobleaching coefficient
photocytotoxicity
cell accumulation

ABSTRACT

Photophysical and *in vitro* photocytotoxicity studies were performed for the photosensitizer Dimegine, a disodium salt 2.4-di(alpha-methoxyethyl)-deuteroporphyrin-IX with very low systemic toxicity. The singlet oxygen and luminescence quantum yield were $\Phi_{\Delta}$ = 0,65 ± 0,06, and $\Phi_f$=0,11 ± 0,01 respectively, and were independent of the excitation wavelength. The photobleaching coefficients for Dimegine dissolved in phosphate buffer (pH 7.4), and DMEM medium at concentration 2 μM/l and in phosphate buffer (pH 7.0) at concentration 10 μM/l were $16{\cdot}10^{-5}$, $9{\cdot}10^{-5}$ and $2{\cdot}10^{-5}$ respectively. *In vitro* cellular distribution and photocytotoxicity was studied in two human (*U87* – primary glioblastoma and *HT1376* – bladder cancer) and two rat cell lines (*RG2* – glioma, and *AY27* – bladder carcinoma). Fluorescence microscopy analysis shows primary Dimegine accumulation as small fluorescent inclusion bodies around the nuclei, suggesting an apoptotic over a necrotic cell death mechanism. The PDT efficacy was slightly higher for the rat cell lines over the human-derived cell lines, with $LD_{50}$ values of 2,5 μM/l, 2.8 μM/l, 4.5 μM/l, 2.8 μM/l using 530 nm excitation wavelength for *AY27*, *RG2*, *HT1376* and *U87* respectively, and 1.8 μM/l, 2 μM/l, 5 μM/l, 2.4 μM/l using 625 nm excitation wavelength for *AY27*, *RG2*, *HT1376* and *U87* respectively. Comparison to literature data showed that Dimegine demonstrated improved phototherapeutic characteristics comparing to PpIX-mediated PDT.

## 1. Introduction

Photodynamic therapy (PDT) is a selective and hence highly effective therapeutic method for malignant tumours treatment [1–6]. It is based on oxidative stress generated inside the cells via a light-absorbing photosensitizer (PS). Selectivity is provided by an affinity of the sensitizer to the malignant tissues and cells, and its preferential uptake by tumor cells versus normal tissues. This allows generating cell-toxic reactive oxygen species (radicals, type I reaction) or singlet oxygen, $^1O_2$ (type II reaction)) selectively within the target tissue with no or minimal destruction of normal cells.In addition to direct oxidative stress, PDT can cause an immune response and therefore disturb the tumour growth; both can elicit a positive impact on the treatment efficacy [7–10].

Photodynamic therapy is now used to treat various skin and gastrointestinal and other cancers, including but not limited to bladder, lung and brain cancers [6,11,12] with a variety of PSs. It is also used for the treatment of tumors of hard-to-reach organs like ENT- organs and the pancreas [5,13].

Despite these various approvals, a current limitation that restricts further exploitation of PDT is the lack of highly selective and low-toxic photosensitizers since complete tumour tissues selectivity cannot be achieved for currently available PSs. This reduces the effectiveness of photodynamic therapy and is fueling the search and study of novel promising photosensitizers.

Currently approved photosensitizers and those being investigated have a range of pharmacological, physical and chemical properties. The key attributes for an "ideal" photosensitizer are well-known and should be as following: preferential accumulation in the target neoplastic tissue, effective singlet oxygen and other reactive oxygen species generation with a high triplet formation quantum yield ($\Phi T \geq 0.5$) and high singlet oxygen quantum yield ($\Phi\Delta \geq 0.5$), minimal dark toxicity,

* Corresponding author.
*E-mail address:* dav3005@rambler.ru (A.V. Dadeko).

https://doi.org/10.1016/j.pdpdt.2018.11.006
Received 13 September 2018; Received in revised form 24 October 2018; Accepted 5 November 2018
Available online 06 November 2018

simple and stable drug formulation, good solubility in biological media allowing systemic administration, and activation by long-wavelength light in the optical therapeutic window (600-800 nm) among others [14].

Some of the basic characteristics of a PS are of chemical nature, such as its hydrophilic/hydrophobic balance, which has a significant impact on its ability to penetrate into the cells [15]. Since the dominant cytotoxic agent, singlet oxygen $^1O_2$ can diffuse in cells over approx. 20-100 nanometers, depending on the microenvironment, the subcellular localization of the PS defines the cellular targets that are subjected to the PDT insult. Cellular organelles, in particular, mitochondria, often attract PS due to the charges they carry. Such localization leads to cell death without the possibility of cellular regeneration (apoptotic mechanism) [1,16]. In contrast, in the case of PS localization within the cell membrane or cytoplasm, regeneration of a cell is possible (necrotic mechanism) [1,16]. Well documented advantages of apoptotic cell death mechanism are the lack of strong local inflammatory reaction and the possibility of launching a cascade of reactions leading to the destruction of the tumour cells, e.g. by the bystander effect [17]. Modern PDT protocols are often based on induction or enhancement of apoptosis of cancer cells [18]. Mitochondria play a central role in the initiation of apoptotic cell death in eukaryotes [19] and hence present a preferable target for PS in PDT.

One class of photosensitizers studied in detail are porphyrins, as they possess low dark toxicity and do not show pharmacological interactions with other drugs, improving the safety of PDT procedures in patients receiving other disease-associated medications [20].

Our present study extends prior results on disodium salt 2.4-di (alpha-methoxyethyl)-deuteroporphyrin-IX, named Dimegine, an amphiphilic PS. The chemical structure of Dimegine is presented in Fig. 1. Recently, the qualitative comparison of Dimegine with Photoditazine and Radachlorin, both Chlorine e6 class photosensitizers, has been made. The results show that Dimegine has a slightly higher fluorescence intensity and singlet oxygen generation rate for irradiation with green light. These parameters of Dimegine were lower compared to those of Photoditazine and Radachlorin when excitation with red light was used. Despite this, a higher photostability of Dimegine comparing to Photoditazine and Radachlorin compensates its lower fluorescence yield and rate of singlet oxygen generation during red-light irradiation and therefore allows for the delivery of an overall higher dose of photons [21]. It was also shown that Dimegine has a faster clearance from tissues and lower systemic toxicity than Photoditazine and Radachlorine [22], providing additional benefit for the patient regarding systemic toxicity, in particular, caused by solar irradiation.

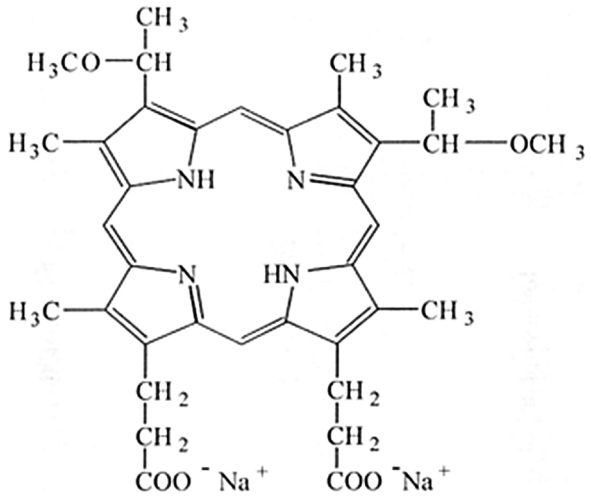


**Fig. 1.** Chemical structure of disodium salt 2.4-di (alpha-methoxyethyl)-deuteroporphyrin-IX (Dimegine).

However, to assess the overall clinical potential of Dimegine and allow simulations of the PDT treatment effects [23–25], absolute values of the singlet oxygen and luminescence quantum yields, as well as photobleaching coefficient, are required. In particular, for the development and optimization of treatment protocols, it is important to choose good starting values for the optimal doses of both PS and light irradiation in pre-clinical and clinical studies. While some cytotoxicity studies of Dimegine have been published, no data exist to date about its cellular distribution and toxicity in various cell lines.

As indicated above, effective PS's should provide a quantum yield of 0.5 or higher. This study aims therefore to determine the singlet oxygen quantum yield for Dimegine to assess its applicability in photodynamic therapy. In addition to photodynamic therapy, a PSs can also be of use, in fluorescent diagnosis, i.e. to localize a tumour's boundaries via its fluorescence emission, following optical excitation. Hence, its fluorescence quantum yield also needs to be determined. A high fluorescence quantum yield suggests the ability of given PS to be used for 3D tumour localization using novel imaging techniques such as spatial domain fluorescence imaging [26].

The PS's photobleaching rate depends on its aggregation state and the microenvironment. The polarity and pH of the medium are also important factors determining the rate of photodegradation [27]. The addition of an organic solvent to the aqueous buffer solution increases the resistance of the photosensitizer to degradation upon light irradiation [28]. Bleaching of dyes can be caused by photochemical reactions of oxidation, reduction, and degradation (photolysis). Hence, the bleaching rate needs to be determined for multiple solvents.

Determination of the photophysical parameters of Dimegine follows standard published protocols [29,30,31].

## 2. Materials and methods

### 2.1. Photosensitizers and chemicals

Lyophilized Dimegine was obtained from PHARMZASCHITA of FMBA (Khimki, Moscow region, Russia,). Methylene Blue was purchased from the Open Joint Stock Company "Vecton," (Saint Petersburg, Leningrad region, Russia, CAS # 61-73-4) and used as reference PS due to its high $^1O_2$ quantum yield [32]. Protoporphyrin IX (PpIX) was obtained from Sigma-Aldrich (Mississauga, Ontario, #553-12-8).

L-Tryptophan was purchased from Sigma-Aldrich (Moscow, Russia, CAS #73-22-3), DMSO was purchased from ThermoFisher (Waltham, Massachusetts, USA #S36002), DMEM media, Fetal Bovine Serum, Glutamine, and Penicillin/Streptomycin were purchased all from Life Technologies (Carlsbad, CA, USA), PrestoBlue from (Invitrogen Canada Inc., # A13261)

### 2.2. Cell lines

Glioma and bladder cancer cell lines, one each of human (*U87*, ATCC #HTB-14, and *HT1376*, ATCC #CRL-1472) and rat (*RG2* and *AY27*) origin were used in this study.

The cell lines were maintained as reported in the literature. Briefly, *U87* [33,34] and *RG2* [35] were grown in DMEM supplemented with 10% Fetal Bovine Serum, 2 mM glutamine, and Penicillin/Streptomycin (all from Life Technologies, Carlsbad, CA, USA). *AY27* [36] and *HT1376* [37] were cultured similarly without glutamine. All cell lines were maintained at 37 °C at 5% $CO_2$. The medium used for cell cultivation contained phenol red; however, phenol red-free medium was used for PDT and the PrestoBlue metabolic survival assay.

### 2.3. Determination of the singlet oxygen quantum yield

To determine Dimegine's singlet oxygen quantum yield ($\Phi_\Delta$) Methylene Blue in phosphate buffer saline pH 7.0 was used as standard

($\Phi_\Delta$ = 0.52) [32].

Dimegine was dissolved in phosphate buffer saline at pH 7.0. The selected PS concentrations ($0.45{\cdot}10^{-4}$M·L$^{-1}$ for Methylene Blue and $0.5{\cdot}10^{-4}$ M·L$^{-1}$ for Dimegine) compensated for differences in the molar extinction coefficient at the irradiation wavelength (525 nm) 3777 L M$^{-1}$ cm$^{-1}$ and 3400 L M$^{-1}$ cm$^{-1}$ for Methylene Blue and Dimegine, respectively. This resulted in the same absorbed photon number per mL.

Tryptophan solution, (73 μM), was used as a chemical trap, which transforms into endoperoxide with different absorption spectrum upon interaction with singlet oxygen. The decrease of tryptophan concentration, therefore, depends on the efficacy of singlet oxygen generation for given experimental conditions. The amount of singlet oxygen generated in the course of irradiation for each PS was evaluated by the decline of tryptophan's absorption measured at 218 nm. The Dimegine and Methylene Blue solutions containing tryptophan were irradiated at 80 mWcm$^{-2}$ with a 525 nm laser diode for 1 minute. Six cycles of irradiation, 10 secs each, were used in the experiments. After 10, 30 and 60 seconds (cycles 1, 2 and 6), the tryptophan absorbance was quantified using a Shimadzu UV-3600 (Shimadzu Corporation, Japan) spectrophotometer, whereby the excitation power was < 1 mW. The tryptophan concentrations at specific time points were plotted against the irradiation time. To calculate the quantum yield of singlet oxygen generation ($\Phi_{PS}$), equation (1) was used [29]:

$$\Phi_{PS} = \frac{(c_0 - c_t)N_a V_R}{(1 - 10^{-D})AIt} \quad (1)$$

Here $c_0$ and $c_t$ are the tryptophan concentrations before and after irradiation, respectively, $V_R$ is the reaction volume, $t$ is the irradiation time per cycle (10 sec), $D$ is the absorbance of the sensitizer at the irradiation wavelength, $A$ is the irradiated area, $I$ is the intensity of light and $N_a$ is Avogadro's constant. Due to interference of the spectra of tryptophan and endoperoxide, we considered for calculations the time point 10 sec when the amount of endoperoxide was low, and its impact on the optical density was not pronounced.

The quantum yield of Dimegine-driven singlet oxygen generation was calculated according to equation (2), obtained from equation (1):

$$\Phi_{\Delta D} = \Phi_{\Delta MB}\frac{(c_{0D} - c_{tD})}{(c_{0MB} - c_{tMB})} \quad (2)$$

Here $c_0$ and $c_t$ are the tryptophan concentrations before and after irradiation for Dimegine (*D*) and Methylene Blue (*MB*), respectively, with $\Phi_{\Delta D}$ and $\Phi_{\Delta MB}$ being their singlet oxygen quantum yields, considering that $\Phi_{\Delta MB}$ = 0.52 [32].

### 2.4. Fluorescence quantum yield and photobleaching coefficient determination

Protoporphyrin IX (PpIX) was used as a reference compound to determine Dimegine's fluorescence quantum yield. Solutions of PpIX (20 μM) in DMSO and Dimegine (0.5 μM) in PBS were prepared. These solutions are of equal optical density at 404 nm, the wavelength further used for fluorescence excitation. Roughly, this suggests an equal number of excitation photons absorbed by equal volumes of these solutions. The fluorescence spectra were recorded on a Shimadzu RF-5301PC fluorescent spectrometer using 404 nm light for excitation.

The areas under the emission spectrum curves were integrated, and the results of three independent experiments were averaged. Dimegine's fluorescence quantum yield was calculated as the ratio of the two areas taking into account the refractive indices of solvents and the fluorescence quantum yield of PpIX [38] as represented in equation (3) [39]:

$$\Phi_{fD} = \Phi_{fPpIX}\frac{S_D n_D^2}{S_{PpIX} n_{PpIX}^2} \quad (3)$$

where $S_D$ and $S_{PpIX}$ are the integrated areas under the emission spectra of the Dimegine and PpIX respectively, $n_D$ and $n_{PpIX}$ are the refractive indices of solvents in which Dimegine and "Protoporphyrin IX" were dissolved, respectively, and $\Phi_{fD}$ and $\Phi_{fPpIX}$ are their fluorescence quantum yields, given that $\Phi_{fPpIX}$ = 0.16 [38].

To determine Dimegine's photobleaching coefficient, a 2 μM solutions in either PBS pH 7.4 or DMEM medium with a molar extinction coefficient of 4221 l*M$^{-1}$*cm$^{-1}$ at 530 nm were prepared and irradiated for 5 min at 250 mWcm$^{-2}$. The resulting fluorescence exited at 395 and registered at 635 nm was measured every 30 seconds using a Gemini EM Microplate Reader (Molecular Devices, San Jose, USA). Dimegine's 10 μM solution in PBS pH 7.0 with a molar extinction coefficient of 101100 l*M$^{-1}$*cm$^{-1}$ was irradiated for 1 min at 250 mWcm$^{-2}$ using 400 nm light. Previously we have optimized these parameters [21]. At these conditions, the irradiation power density corresponds those recommended for bladder and skin cancers [40,41] Changes in PS concentration were registered every 10 seconds by measuring the optical density of Dimegine at its absorption peak at 392 nm using the Shimadzu UV-3600 spectrophotometer.

The resulting fluorescence and absorbance intensities were used to determine the photobleaching coefficient by equation (4) [42].

$$\Phi_D = \frac{\frac{(D_0 - D)}{D_0}CN_A V}{N_q} \quad (4)$$

where $D_0$ and D are the optical absorption of the photosensitizer before and after irradiation. C is the concentration of the photosensitizer in the solution before irradiation; $N_A$ is the Avogadro constant, V is the volume of the solution, Nq is the number of photons absorbed by the solution, defined as:

$$N_q = \frac{(1 - 10^{-D})I\lambda t}{hc} \quad (5)$$

where D is the optical density of the irradiated solution at the irradiation wavelength, I is the radiation power density on the sample, λ is the wavelength of the irradiating light, t is the irradiation time in seconds, c is the speed of light, and h is the Planck constant.

### 2.5. Photocytotoxicity

For photocytotoxicity experiments, the 4 cell lines (*AY27*, *HT1376*, *U87* and *RG2*) in DMEM were seeded one day prior to PDT light activation, in 96-well microtiter plates at a density of 10,000 cells per well and kept in an incubator for 16 hours at 37 °C in 5% $CO_2$. Cells were incubated with either 10, 5, 2, 1, 0.5 or 0.1 μg ml$^{-1}$ of Dimegine for 3 hours. Cultivation medium was used instead of Dimegine in control wells. After 3 hours, the medium was replaced with phenol red-free DMEM. One 96 well plate was irradiated using a 530 nm diode laser array for 60 sec at 250 mWcm$^{-2}$ to achieve a radiant exposure of 15 Jcm$^{-2}$, and the second plate was irradiated using 625 nm emitting laser arrays for 300 sec at 220 mWcm$^{-2}$ to achieve a radiant exposure of 66 Jcm$^{-2}$ (both TLC 3000, Theralase Inc. Toronto, Canada)(molar extinction coefficients of $10^{-5}$ M/l Dimegin's concentration were 4221 l*M$^{-1}$*cm$^{-1}$ and 879 l*M$^{-1}$*cm$^{-1}$ at 530 nm and 625 nm respectively). The difference in radiation exposures provides the identical amounts of photons absorbed by Dimegine upon irradiation with green (530 nm) and red (625 nm) light, considering the difference in the molar extinction coefficients of Dimegine at these wavelengths and the quantum energy of the photons. A separate 96-well plate was kept in the dark, serving as a drug-only control. All plates were kept for the same duration outside the incubator. Following the light irradiation, the microtiter plates were returned into the incubator for the next 22 hours [33,34,35], followed by incubating the cells for one hour with PrestoBlue (1:10 dilution of the stock solution) and further measuring of the fluorescence at 600 nm using a Gemini EM Microplate fluorescence reader. For each cell line, the intensity of the fluorescence was plotted against the concentration of Dimegine, and the 50% lethal dose ($LD_{50}$)

values were calculated using GraphPad Prism software. All experiments were performed in triplicates.

### 2.6. Luminescent microscopy

#### 2.6.1. Study of cellular localization of Dimegine

$5 \times 10^4$ cells of either *AY27*, *HT1376*, *U87* or *RG2* line were seeded into Lifecell imaging chamber (Ibidi, München, Germany) and allowed to adhere for 24 hrs in $CO_2$- incubator. Cells were treated as described above, using a Dimegine concentration of 2 μg ml$^{-1}$. After 3 hours of incubation, the medium was changed to phenol red-free DMEM for imaging. Fluorescence micrographs were collected with a Zeiss Confocal Micrographs (Zeiss LSM700, Jena, Germany) using a 63× objective and 405 nm excitation. Fluorescence at 465 nm was recorded via a 20 μm pinhole.

### 2.7. Statistical treatment of results

All results were presented as mean ± standard error of the mean. The efficacy of different wavelengths was compared by an unpaired *t*-test. The susceptibility of different cell lines to PDT was compared by one-way ANOVA. The values of 50% lethal dose ($LD_{50}$) of Dimegine were calculated using GraphPad Prism software.

## 3. Results

### 3.1. Photophysical properties of Dimegine

To determine Dimegine's $\Phi_\Delta$, the tryptophan concentration characterizing singlet oxygen generation was plotted against the irradiation time for Methylene Blue and Dimegine (Fig.2). It could be noticed that the concentration regression rate was not constant during irradiation, *i.e.* the regression is not linear. This is due to the overlap of the endoperoxide and tryptophan absorption spectra, as shown for Methylene Blue in Fig. 3. Hence, to determine $\Phi_\Delta$ only first 10 sec irradiation interval was utilized to minimize the effect of endoperoxide accumulation. Using the slopes of the regression lines and correcting for the known $\Phi_\Delta$ = 0.52 of Methylene Blue in ethanol [32] (equation 2), the resulting singlet oxygen quantum yields for Dimegine in PBS (pH = 7.0) was calculated as $\Phi_{\Delta D}$ = 0.65 ± 0.06.

The fluorescence emission spectra of PpIX and Dimegine are shown in Fig. 4. Taking the ratios of the area under the emission curves, the refractive indices of PS solutions and the known PpIX fluorescence quantum yield ($\Phi_{fPpIX}$ = 0.16) [38], fluorescence quantum yield for Dimegine dissolved in PBS of pH7.4 was determined as $\Phi_f$

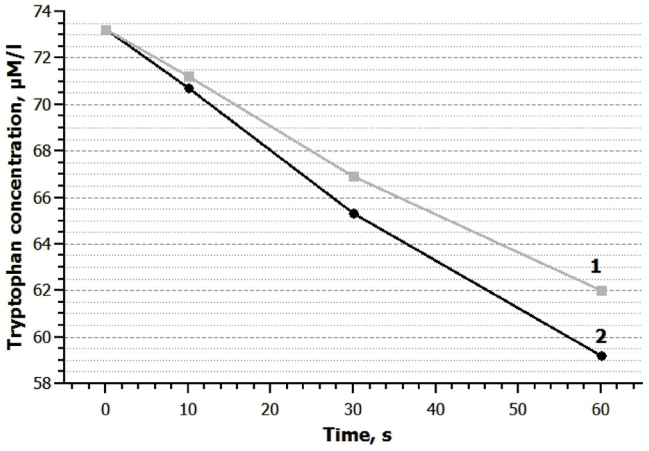


**Fig. 2.** Dynamics of tryptophan concentration in Methylene Blue (1) and Dimegine (2) solutions upon irradiation at 80 mWcm$^{-2}$ with a 525 nm laser diode.

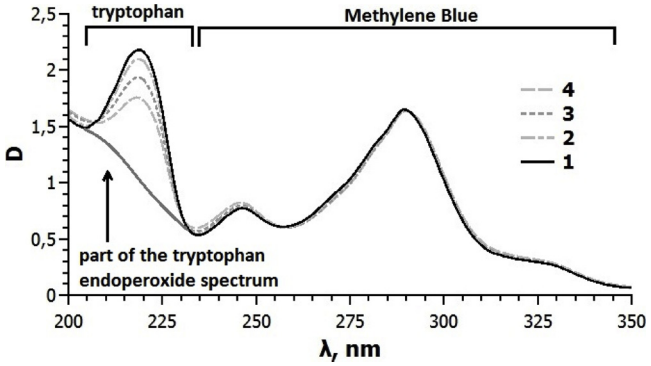


**Fig. 3.** Changes in absorbance spectrum of Methylene Blue containing tryptophan dissolved in phosphate buffer pH 7.0 during irradiation at 80 mWcm$^{-2}$ with a 525 nm laser diode. Methylene Blue and tryptophan concentrations are $0.45 \cdot 10^{-4}$M·L$^{-1}$ and $7.3 \cdot 10^{-5}$M·L$^{-1}$ respectively. Lines 1,2,3,4 correspond to 0, 10, 30 and 60 sec of irradiation respectively. For comparison, part of tryptophan endoperoxide spectrum is presented to make visible the interference of tryptophan and tryptophan endoperoxide spectra (absorbance peak of tryptophan endoperoxide at 200 nm is not shown).

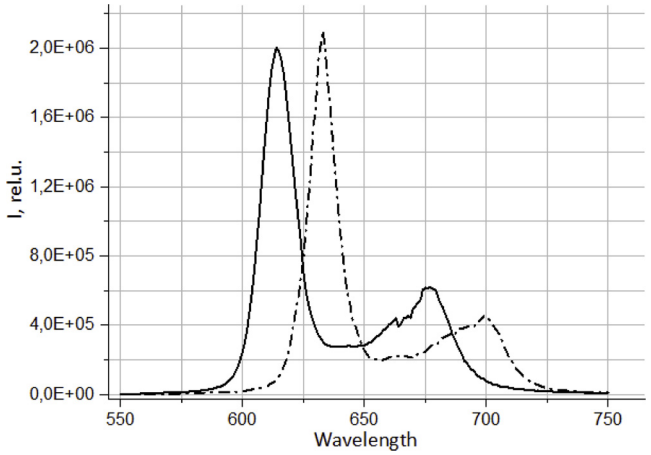


**Fig. 4.** Fluorescence spectra of PpIX (dashed) and Dimegine (solid) following excitation with λ = 404 nm.

$_D$ = 0.11 ± 0.01.

Dimegine concentration change during irradiation was used to determine the photobleaching coefficient according to equation (4). For 2 μM Dimegine dissolved in PBS pH 7.4 and DMEM medium, photobleaching coefficients were $\varphi_{buf7.4} = 16 \cdot 10^{-5}$ and $\varphi_{med} = 9 \cdot 10^{-5}$ respectively, and for 10 μM solution in PBS pH 7.0 – $\varphi_{buf7.0} = 2 \cdot 10^{-5}$ [43].

### 3.2. Photocytotoxicity assay

To assess the cytotoxicity of Dimegine with and without irradiation, the viability of cells of four lines of different genesis was studied. Figs. 5 and 6 show the cell survival rates for the four Dimegine-sensitized cell lines irradiated by either 530-nm (green) or 625-nm (red) light. The $LD_{50}$ of Dimegine for each of the studied cell lines are presented in Table 1. It can be noted that to destroy the same amount of malignant cells *RG2* and *U87*, the required concentration of Dimegine is 268 and 222 times lower than that of ALA indused PPIX, correspondingly.

For all cell lines, the cytotoxic effect of Dimegine without irradiation (dark toxicity) did not exceed 11% (Fig.7) for all tested concentrations. Among four cell lines used in the experiments, *HT1376* derived from human bladder tumor was the most resistant to the Dimegine-based PDT. Indeed, when irradiated with green light (530 nm) in the presence of 2 μg/mL Dimegine a significantly lower cell death rate was noted compared to *U87*, *RG2* and *AY27* cells ($p = 0.0381$;

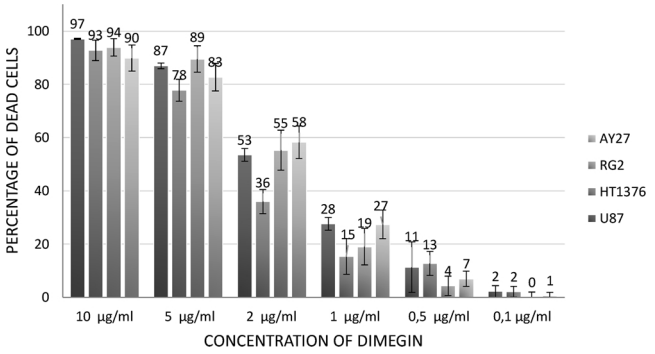


**Fig. 5.** Photocytotoxic effect of Dimegine in different cell lines under light irradiation with λ = 530 nm, source power – 250 mW/cm$^2$. M ± SE, n = 6.

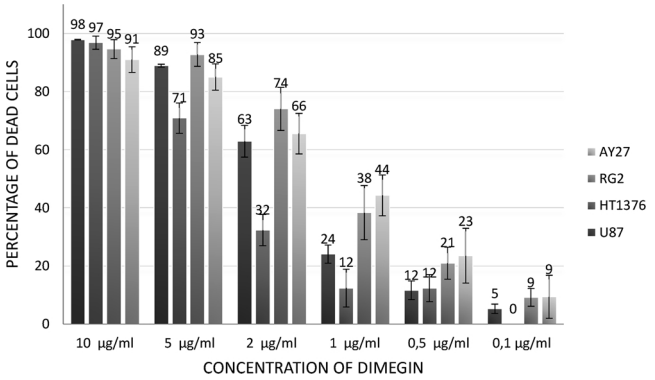


**Fig. 6.** Photocytotoxic effect of Dimegine in different cell lines under light irradiation with λ = 625 nm, source power – 250 mW/cm$^2$. M ± SE, n = 6.

**Table 1**
The $LD_{50}$ values of Dimegine and **ALA induced PpIX** in different cell lines (M ± SE, n = 3).

| Photosensitizer | Dimegine | | ALA-induced PpIX |
|---|---|---|---|
| Irradiation conditions | λ = 530 nm at 250 mW/cm$^2$ | λ = 625 nm at 227 mW/cm$^2$ | λ = 635 nm at 156 mW/cm$^2$ |
| Cell line | | | |
| AY27 | 2.5 μM/l | 1.8 μM/l | |
| RG2 | 2.8 μM/l | 2 μM/l | 535 μM/l[a] |
| HT1376 | 4.5 μM/l | 5 μM/l | |
| U87 | 2.8 μM/l | 2.4 μM/l | 533 μM/l[a] |

[a] Calculated from [52]

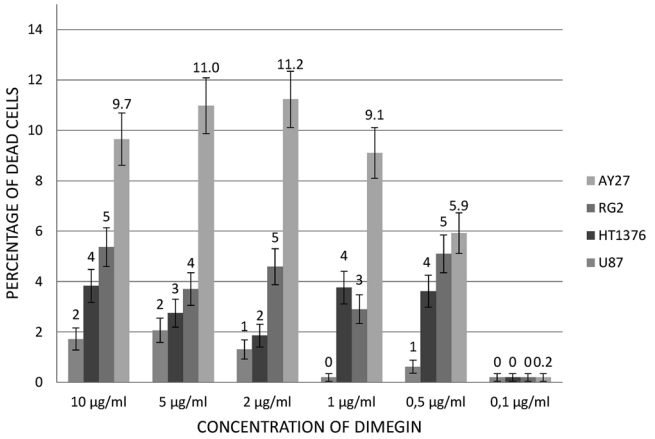


**Fig. 7.** Dark toxicity effect of Dimegine in different cell lines without irradiation. M ± SE, n = 6.

0.0098 and 0.0007 correspondingly). At 5 μg/mL Dimegine was also less effective in *HT1376* than *RG2* cells ($p$ = 0.0175).

These differences were even more pronounced for red treatment light (625 nm). At 1.0 μg/mL Dimegine, *HT1376* cells were two- to four times more resistant to PDT than *AY27* and *RG2* cells ($p$ = 0.0052 and 0.0452). This line was also significantly less susceptible than all other cell lines at 2.0 ($p$ < 0.0001; < 0.0001; and 0.0012) and 5.0 μg/mL Dimegine ($p$ = 0.0004; < 0.0001 and 0.0011 comparing to *AY27*, *RG2* and *U87* cells correspondingly).

When the efficacies of two wavelengths were compared, it was found that the 625 nm wavelength (red light) tends to be slightly more effective. Indeed, for RG2 cells at 0.5 and 2.0 μg/mL Dimegine, the cell death rate was significantly higher after red irradiation compared to green one ($p$ = 0.0198 and 0.0282 correspondingly). For *U87* cells the same tend was observed at Dimegine concentrations of 0.1 and 2.0 μg/mL ($p$ = 0.0334 and 0.0005 correspondingly). *AY27* and *HT1376* cells did not demonstrate statistically significant selectivity in favor of red light comparing to the green one. The trend, however, was observed for all cell lines and Dimegine concentrations (Figs.5 and 6).

### 3.3. Luminescent microscopy

To assess the cellular distribution of Dimegine, we incubated the cells of four lines used with a 2 μg/ml Dimegine solution and studied the cells by fluorescent microscopy as presented in Fig. 8. At 3 hours post Dimegine exposure we observed punctate fluorescent structures surrounding the nucleus, suggesting mitochondria or the rough endoplasmic reticulum as sites of Dimegine accumulation. The spatial distributions of the fluorescence were similar between all four cell lines independently of species.

## 4. Discussion

While various photosensitizers have been approved for clinical application, the worldwide increase of cancer cases still motivates the development of novel photosensitizers for tumour treatment. Owing to the use of non-toxic photosensitisers that accumulate preferentially within tumor cells, PDT is a minimally invasive way of treatment for neoplasms. One way to provide selectivity of PS's tissue accumulation in favor of tumor cells is the application of prodrugs, i.e. chemical compounds that are further converted to photodynamically active PS [44]. The only clinically approved PS precursor is δ-aminolevulinic acid (ALA). Upon cell penetration, conjugation of eight ALA molecules by the cellular enzymatic machinery results in the synthesis of PpIX. As the tumor cells possess a higher level of metabolism in general, and higher expression of PpIX-synthesizing enzymes in particular, the photodynamically active PpIX accumulates preferentially in the tumor. Moreover, cancer cells often have dysregulated enzymes converting PpIX to heme that results in additional accumulation of PpIX in tumor cells [45] comparing to normal ones where PpIX is effectively converted to heme. Although these features are obvious advantages of ALA-based PDT, they at the same time make it difficult to control the accumulation of PpIX within various tumors differing in their level of activity of numerous enzymes of heme biosynthesis and PpIX metabolism. This, in turn, results in a wide range of PpIX concentrations in different tumors and low reproducibility in the calculation of the optimal light exposure time and radiant exposure of fluence in the course of PDT.

In this regard, the anti-cancer activity mechanisms of Dimegine differs from that of ALA-induced PpIX, as Dimegine is not a pro-drug and hence does not depend on a cell's ability to synthesize the photodynamically active compounds as for ALA and its various derivatives towards the synthesis of PpIX. Dimegine, therefore, is not a subject to dysregulation of the heme biosynthesis pathway and accumulates within cells independently of the activity of their heme-synthesizing enzymes. This, on the one hand, allows to control Dimegine's

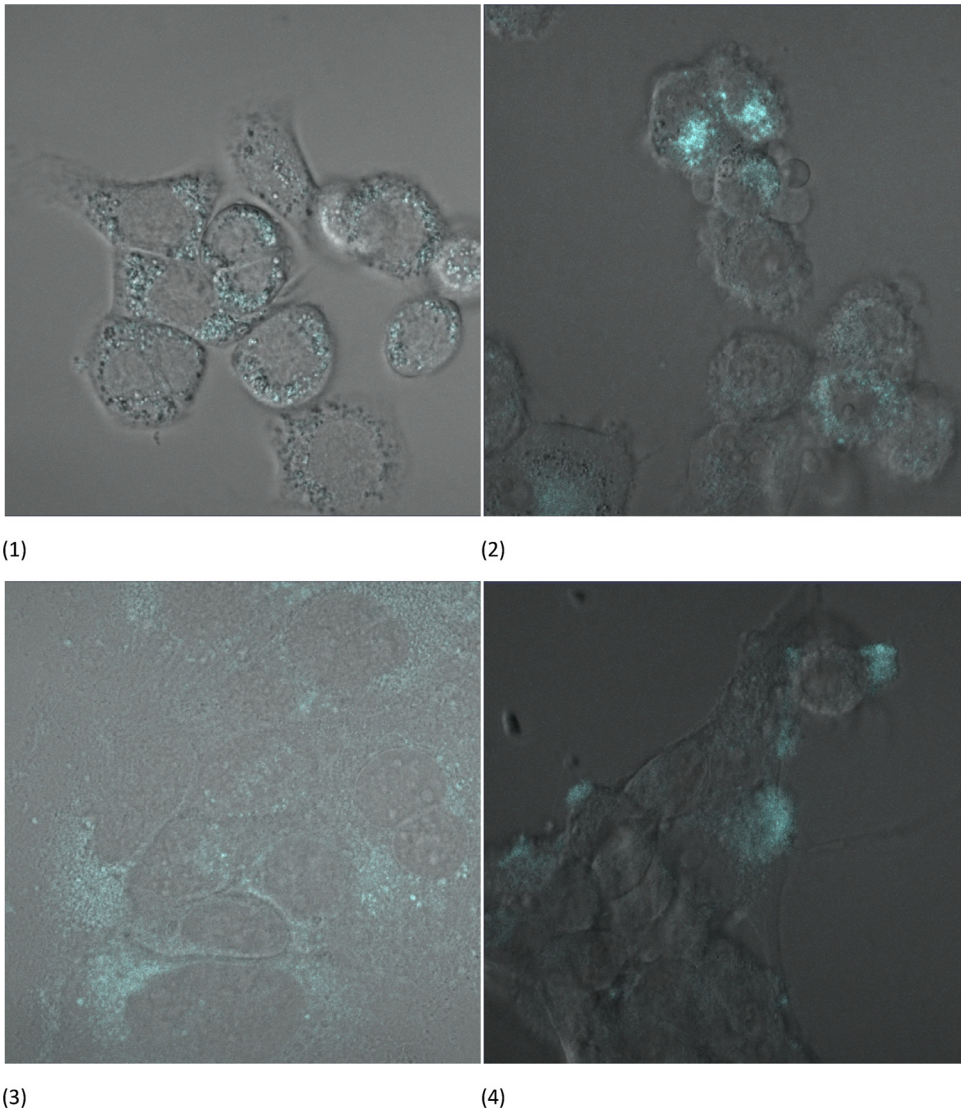


**Fig. 8.** Subcellular localization of Dimegine (2 μg/ml solution) in the cells of *AY27*(1), *U87*(2), *HT1376*(3), *RG2*(4) lines. Excitation wavelength 465 nm. The cells were exposed to 2 μg/ml Dimegine for 3 hours following by fluorescent microscopy assay. Dimegine was observed as punctate fluorescent structures surrounding the cell nuclei. Magnification × 63.

concentration in the tumor and calculate the dose of light uniformly for PDT of the target volume. On the other hand, this raises the selectivity question of Dimegine's towards its accumulation in tumor cells comparing to healthy tissues. Current data suggest that Dimegine accumulates in tumor cells at concentrations 16-30 times higher than in normal cells [46].

Dimegine was shown to have lower dark toxicity and faster system clearance than some Chlorine e6-based photosensitizers that are currently under clinical investigation [22].

The results published to date on Dimegine describe only its qualitative photophysical and photobiological data [21,22,47]. However, to optimize clinical PDT treatment protocols and enable personalized cancer therapies, quantitative photophysical and photochemical characteristics are required. In the present study, the photophysical parameters, such as singlet oxygen quantum yield, fluorescence quantum yield and photobleaching coefficient are determined. In addition to photobiological data, we determined the $LD_{50}$ of Dimegine in four different cell lines and its subcellular localization.

The singlet oxygen quantum yield of Dimegine in PBS is as high as 0.65. This is comparable to the $\Phi_\Delta$ values of ALA-induced PpIX in DMSO (0.56) [38], or Chlorine e6 in DMSO (0.65) [38], but higher than that of Photofrin in methanol (0.25) [48] and lower than $\Phi_\Delta$ of benzoporphyrin derivative monoacid ring A (BPD-MA) in methanol (0.78) [49]. Since novel photosensitizers have been reported with a $\Phi_\Delta$ similar to each other in solutions [50], optical monitoring of their accumulation in cells and tissues is critical for their development and further clinical application.

The fluorescence quantum yield of 0.11 is high enough to encourage the use of Dimegine also in photodynamic diagnostics once the desired selectivity between normal and cancer tissues is achieved. Other photosensitizers in current use for photodiagnostics such as PpIX and Chlorine e6 dissolved in DMSO have fluorescent quantum yields of 0.16 and 0.19, respectively [38].

The photobleaching coefficients of Dimegine at 2 μM concentration, are $\varphi_{buf7.4} = 16{\cdot}10^{-5}$ in buffer solution (pH 7.4) and $\varphi_{med} = 9{\cdot}10^{-5}$ in DMEM medium, and $\varphi_{buf7.0} = 2{\cdot}10^{-5}$ at 10 μM in phosphate buffer solution (pH 7.0) are also comparable to the photobleaching coefficients of Hematoporphyrin – $4.7{\cdot}10^{-5}$, Photofrin II – $5.4{\cdot}10^{-5}$ and Uroporphyrin – $2.8{\cdot}10^{-5}$ [43]. Decreased photobleaching rate of higher Dimegine concentration could be explained by its aggregation. Photodestruction of Dimegine also depends on the solvent but remains rather low compared to chlorine-based photosensitizers (photobleaching coefficient for

Photoditazine – $\varphi_{buf7.0} = 27 \cdot 10^{-5}$) because of its high symmetry of the porphyrin core [28].

The PDT efficacy of Dimegine was compared to that of ALA-induced PpIX for the four cell lines (Table 1). It can be noted that to destroy the same amount of malignant cells *RG2* and *U87*, the required concentration of Dimegine is more than two orders of magnitude lower than that of ALA-induced PpIX, indicating the possibility of using lower doses of Dimegine for systemic (intravenous) administration to achieve a similar therapeutic effect. This difference could be due to the high photostability of Dimegine and its specific subcellular localization [51].

*HT1376* cell line was proven to be less sensitive to the combined action of irradiation and Dimegine than other cell lines using both green and red therapeutic light. The better photodynamic treatment results for rat-derived neoplastic cells compared to those with human cells is intriguing and should be further investigated. Low dark toxicity of Dimegine characterizes it as a good photosensitizer for clinical applications.

The study of the sub-cellular distribution of Dimegine showed that it accumulates within cells as numerous small inclusions located around cell nuclei. Dimegine accumulation in mitochondria has been confirmed in the study of Fickweiler et al. [51]. In this study, similarly to our results, the Dimegine fluorescence was localized in membranous structures located extranuclear. It was shown to be colocalized with mitochondria while no association with lysosomes was detected [51]. In this regard, our results are in agreement with others and suggest that binding to mitochondria will results in apoptotic cell death.

## 5. Conclusion

The measured high singlet oxygen quantum yield for Dimegine (0.65) is very promising to continue development of this photosensitizer. The other desired features for an “ideal” PS are also true for Dimegine; including high luminescence quantum yield (0.11) permitting to consider the use of Dimegine for photodiagnostics. The photostability of Dimegine is much higher than that of Photoditazine. The low photobleaching rate will, therefore, allow the use of Dimegine at low concentrations and utilize a higher photon density to reach a therapeutic PDT dose.

Selective Dimegine accumulation in mitochondria has been confirmed in another study [51]. The similarity of the reference data and the obtained results allow us to speculate that the predominant mechanism of cell death in PDT with Dimegine is apoptosis, which positively affects treatment efficiency.

Summarizing the results of the study of photophysical and photocytotoxic properties of Dimegine, we state that this photosensitizer is promising for further development for purposes of photodiagnostics and phototherapy because of its high efficiency and low toxicity. Therefore it can be recommended for clinical trials and subsequent introduction into medical practice.

This research did not receive any specific grant from funding agencies in the public, commercial, or not-for-profit sectors.

## References

[1] M. Kubiak, L. Lysenko, H. Gerber, R. Nowak, Cell reactions and immune responses to photodynamic therapy in oncology, Postepy Higieny i Medycyny Doswiadczalnej 70 (2016) 735–742.
[2] A. Kawczyk-Krupka, A.M. Bugaj, M. Potempa, K. Wasilewska, W. Latos, A. Sieron, Vascular-targeted photodynamic therapy in the treatment of neovascular age-related macular degeneration: Clinical perspectives, Photodiagnosis and Photodynamic Therapy 12 (2) (2015) 161–175.
[3] P. Agostinis, K. Berg, K.A. Cengel, T.H. Foster, A.W. Girotti, S.O. Gollnick, S.M. Hahn, M.R. Hamblin, A. Juzeniene, D. Kessel, M. Korbelik, J. Moan, P. Mroz, D. Nowis, J. Piette, B.C. Wilson, J. Golab, Photodynamic therapy of cancer: an update, CA Cancer Journal For Clinicians 61 (4) (2011) 250–281.
[4] C.A. Morton, R.M. Szeimies, A. Sidoroff, L.R. Braathen, European guidelines for topical photodynamic therapy part 1: treatment delivery and current indications - actinic keratoses, Bowen’s disease, basal cell carcinoma, Journal of the European Academy of Dermatology and Venereology 27 (5) (2013) 536–544.
[5] C.E. Silver, J.J. Beitler, A.R. Shaha, A. Rinaldo, A. Ferlito, Current trends in initial management of laryngeal cancer: the declining use of open surgery, Eur Arch Otorhinolaryngol 266 (9) (2009) 1333–1352.
[6] D.I. Kebalo, V.I. Yermolova, N.P. Miroshnykova, S.M. Pashchenko, O.D. Zvantseva, N.N. Voloshyna, D.Ye Lashtabega, Effectiveness of the photodynamic therapy with photosensitizer for treatment of basal cell skin cancer located on the head, Zaporozhye Medical Journal 5 (2016) 84–88.
[7] M. Korbelik, J. Sun, I. Cecic, Photodynamic therapy-induced cell surface expression and release of heat shock proteins: relevance for tumor response, Cancer Research 65 (3) (2005) 1018–1026.
[8] S.O. Gollnick, L. Vaughan, B.W. Henderson, Generation of effective antitumor vaccines using photodynamic therapy, Cancer Research 62 (6) (2002) 1604–1608.
[9] N.V. Kudinova, T.T. Berezov, Photodynamic therapy of cancer: Search for ideal photosensitizer, Biochemistry (Moscow) Supplement Series B: Biomedical Chemistry 4 (1) (2010) 95–103.
[10] K. Pizova, K. Tomankova, A. Daskova, S. Binder, R. Bajgar, H. Kolarova, Photodynamic therapy for enhancing antitumour immunity, Biomedical Papers 156 (2) (2012) 93–102.
[11] R.R. Allison, Photodynamic therapy: oncologic horizons, Future Oncol 10 (1) (2014) 123–124.
[12] E. Sam, Photodynamic applications in brain tumors: A comprehensive review of the literature, Photodiagnosis and Photodynamic Therapy 7 (2010) 76–85.
[13] G. Shafirstein, D. Bellnier, E. Oakley, S. Hamilton, M. Potasek, K. Beeson, E. Parilov, Interstitial photodynamic therapy—a focused review, Cancers (Basel) 9 (2) (2017).
[14] J.B. Josefsen, R.W. Boyle, Photodynamic Therapy and the Development of Metal-Based Photosensitisers, Met Based Drugs. (2008), https://doi.org/10.1155/2008/276109.
[15] H. Mojzisova, S. Bonneau, D. Brault, Structural and physico-chemical determinants of the interactions of macrocyclic photosensitizers with cells, European Biophysics Journal With Biophysics Letters 36 (8) (2007) 943–953.
[16] J. Soriano, I. Mora-Espí, M.E. Alea-Reyes, L. Pérez-García, L. Barrios, E. Ibáñez, C. Noguésa, Cell Death Mechanisms in Tumoral and Non-Tumoral Human Cell Lines Triggered by Photodynamic Treatments: Apoptosis, Necrosis and Parthanatos, Scientific Reports. (2017), https://doi.org/10.1038/srep41340.
[17] A.K. Suloglu, E. Karacaoglu, G. Selmanoglu, H. Akel, I.C. Karaaslan, Evaluation of apoptotic cell death mechanisms induced by hypericin-mediated photodynamic therapy in colon cancer cells, Turkish Journal of Biology 40 (3) (2016) 539–546.
[18] J. Lopez, S.W.G. Tait, Mitochondrial apoptosis: killing cancer using the enemy within, Br J Cancer 112 (6) (2015) 957–962.
[19] A.V. Gordeeva, Y.A. Labas, R.A. Zvyagilskaya, Apoptosis in unicellular organisms: mechanisms and evolution, Biochemistry (Mosc) 69 (10) (2004) 1055–1066.
[20] D. Nowis, M. Makowski, T. Stokłosa, M. Legat, T. Issat, J. Gołąb, Direct tumor damage mechanisms of photodynamic therapy, Acta Biochim Pol 52 (2) (2005) 339–352.
[21] A.V. Dadeko, T.D. Murav’eva, A.M. Starodubtsev, S.I. Gorelov, M.V. Dobrun, T.K. Kris’Ko, I.V. Bagrov, I.M. Belousova, G.V. Ponomarev, Photophysical Properties of Porphyrin Photosensitizers, Optics and spectroscopy 119 (4) (2015) 633–637.
[22] S.I. Gorelov, M.V. Dobrun, T.D. Murav’eva, A.M. Starodubtsev, A.V. Kris’ko, V.M. Kiselev, I.V. Bagrov, A.V. Dadeko, S.E. Kolbasov, G.V. Ponomarev, Photophysical properties of dimegin and its preclinical studies, Fotodin. Terap. Fotodiagn 1 (2014) 18.
[23] J. Cassidy, V. Betz, L. Lilge, Treatment plan evaluation for interstitial photodynamic therapy in a mouse model by Monte Carlo simulation with FullMonte, Frontiers in Physics 3 (6) (2015), https://doi.org/10.3389/fphy.2015.00006.
[24] B.C. Wilson, M.S. Patterson, The physics, biophysics and technology of photodynamic therapy, Physics in Medicine and Biology 53 (9) (2008) R61–R109.
[25] S.R. Davidson, R.A. Weersink, M.A. Haider, et al., Treatment planning and dose analysis for interstitial photodynamic therapy of prostate cancer, Physics in Medicine and Biology 54 (8) (2009) 2293–2313.
[26] M. Sibai, C. Fisher, I. Veilleux, et al., Preclinical evaluation of spatial frequency domain-enabled wide-field quantitative imaging for enhanced glioma resection, Journal of biomedical optics 22 (7) (2017), https://doi.org/10.1117/1.JBO.22.7.076007.
[27] P.F.C. Menezes, H. Imasato, V.S. Bagnato, Cl.H. Sibata, J.R. Perussi, Influence of pH on the phototransformation process of photogem, Laser Physics 19 (7) (2009) 1457–1462.
[28] R. Bonnett, G. Martínez, Photobleaching of Compounds of the 5,10,15,20-Tetrakis (m-hydroxyphenyl)porphyrin Series (m-THPP, m-THPC, and m-THPBC), *Org. Lett.* 4 (12) (2002) 2013–2016.
[29] W. Spiller, H. Kliesch, D. Wöhrle, S. Hackbarth, B. Röder, G. Schnurpfeil, Singlet oxygen quantum yields of different photosensitizers in polar solvents and micellar solutions, Journal of porphyrins and phthalocyanines 2 (1998) 145–158.
[30] A.T.R. Williams, S.A. Winfield, J.N. Miller, Relative fluorescence quantum yields using a computer controlled luminescence spectrometer, Analyst. 108 (1983) 1067–1071.
[31] M.B. Levin, M.I. Snegov, A.S. Cherkasov, Photobleaching quantum yields of an aqueous-micellar solution of rhodamine 6g during continuous and pulsed irradiation, Journal of Applied Spectroscopy 47 (5) (1987) 1119–1122.
[32] M.C. DeRosa, R.J. Crutchley, Photosensitized singlet oxygen and its applications, Coordination Chemistry Reviews 233 (2002) 351–371.
[33] M.B. Ian, S. Tamalee, T.T. Anita, E.B. William, L.B. Teresa, J.T. Philip, C. Kevin, Radiosensitization of glioma cells by modulation of Met signalling with the hepatocyte growth factor neutralizing antibody, AMG102, J. Cell. Mol. Med 15 (9) (2011) 1999–2006.
[34] S. Ali, M. Saleh, A. Khurshid, M. Ikram, C. Judy, C. Fisher, L. Lilge, Doxorubicin or Methotrexate exposure followed by Aluminum Phthalocyanine mediated

Photodynamic Therapy provides for effective combination therapy in vitro, Photochemistry and photobiology 17 (2017) A46.
[35] R.F. Barth, Rat brain tumor models in experimental neuro-oncology: The 9L, C6, T9, F98, RG2 (D74), RT-2 and CNS-1 Gliomas, Journal of Neuro-Oncology 36 (1998) 91–102.
[36] S.H. Selman, R.W. Keck, A comparative study of the inhibiting effects of mitomycin C and polyphenolic catechins on tumor cell implantation/growth in a rat bladder tumor model, J Urol. 186 (2) (2011) 702–706, https://doi.org/10.1016/j.juro.2011.03.125.
[37] G. Singh, M. Espiritu, X.Y. Shen, J.G. Hanlon, A.J. Rainbow, In vitro induction of PDT resistance in HT29, HT1376 and SK-N-MC cells by various photosensitizers, Photochem Photobiol. 73 (6) (2001) 651–656.
[38] C.J. Ho, G. Balasundaram, W. Driessen, R. McLaren, C.L. Wong, U.S. Dinish, A.B. Attia, V. Ntziachristos, M. Olivo, Multifunctional Photosensitizer-Based Contrast Agents for Photoacoustic Imaging, Scientific Reports 4 (2014), https://doi.org/10.1038/srep05342.
[39] T.G.B. Souza, M.G. Vivas, C.R. Mendonça, S. Plunkett, M.A. Filatov, M.O. Senge, L. De Boni, Studying the intersystem crossing rate and triplet quantum yield of meso-substituted porphyrins by means of pulse train fluorescence technique, J. Porphyrins Phthalocyan 20 (2016) 282–291.
[40] R.G. Nikitina, M.A. Kaplan, T.G. Morozova, V.V. Drozhzhina, T.V. Epatova, E.Yu. Luk'yanova, Role of Laser Energy Density for Photodynamic Therapy of Radiation Injuries of the Skin, Bulletin of Experimental Biology and Medicine 140 (5) (2005) 558–560.
[41] T.J. Dougherty, C.J. Gomer, B.W. Henderson, G. Jori, D. Kessel, M. Korbelik, J. Moan, Q. Peng, Photodynamic Therapy, JNCI: Journal of the National Cancer Institute 90 (12) (1998) 889–905, https://doi.org/10.1093/jnci/90.12.889.
[42] Yakubovskaya, R.I. et al. Photosensitizers for photodynamic therapy. Patent RU RU2476218, Feb 27 (2013).
[43] J.D. Spikes, Quantum yields and kinetics of the photobleaching of hematoporphyrin, Photofrin II, tetra(4-sulfonatophenyl)-porphine and uroporphyrin, Photochem Photobiol. 55 (6) (1992) 797–808.
[44] M. Wachowska, A. Muchowicz, M. Firczuk, M. Gabrysiak, M. Winiarska, M. Wańczyk, K. Bojarczuk, J. Golab, Aminolevulinic Acid (ALA) as a Prodrug in Photodynamic Therapy of Cancer, Molecules 16 (2011) 4140–4164, https://doi.org/10.3390/molecules16054140.
[45] X. Yang, W. Li, P. Palasuberniam, K.A. Myers, C. Wang, B. Chen, Effects of Silencing Heme Biosynthesis Enzymes on 5-Aminolevulinic Acid-mediated Protoporphyrin IX Fluorescence and Photodynamic Therapy, Photochem Photobiol 91 (4) (2015) 923–930, https://doi.org/10.1111/php.12454.
[46] Davydov EV., Korobov SS. Fluorescent diagnosis of malignant tumor in animals. Patent RU RU2604388C2, Apr 29 (2015).
[47] V.M. Bondarenko, I.V. Alekseev, O.V. Mislavskiĭ, G.V. Ponomarev, Perspectives of disodium salt 2.4-di(1-metoxyethyl)-deuteroporphyrin - IX ("Dimegin") application for photodynamic therapy in non-oncologic cases, Biomed Khim. 60 (3) (2014) 338–347.
[48] M.M. Kim, R. Penjweini, N.R. Gemmell, I. Veilleux, A. McCarthy, G. Buller, R.H. Hadfield, B.C. Wilson, T.C. Zhu, A feasibility study of singlet oxygen explicit dosmietry (SOED) of PDT by intercomparison with a singlet oxygen luminescence dosimetry (SOLD) system, Proc. SPIE 9694, Optical Methods for Tumor Treatment and Detection: Mechanisms and Techniques in Photodynamic Therapy XXV, (2016), p. 9694.
[49] B. Aveline, T. Hasan, R.W. Redmond, Photophysical and photosensitizing properties of benzoporphyrin derivative monoacid ring A (BPD-MA), Photochem. Photobiol. 59 (1994) 328–335.
[50] J. Fong, K. Kasimova, Y. Arenas, P. Kaspler, S. Lazic, A. Mandel, L. Lilge, A novel class of ruthenium-based photosensitizers effectively kills in vitro cancer cells and in vivo tumors, Photochem. Photobiol. Sci. Off. J. Eur. Photochem. Assoc. Eur. Soc. Photobiol. 14 (2015) 2014–2023.
[51] S. Fickweiler, R.-M. Szeimies, C. Abels, G.V. Ponomarev, F. Hofstädter, O.S. Wolfbeis, M. Landthaler, Photosensitization of skin-derived cell lines by Dimegin [2,4-di-(α- methoxyethyl)-deuteroporphyrin IX] in vitro, Photodermatology Photoimmunology and Photomedicine 14 (3-4) (1998) 125–131.
[52] C.J. Fisher, C. Niu, W. Foltz, Y. Chen, E. Sidorova-Darmos, J.H. Eubanks, L. Lilge, ALA-PpIX mediated photodynamic therapy of malignant gliomas augmented by hypothermia, PLOS ONE 12 (7) (2017), https://doi.org/10.1371/journal.pone.0181654.